HIGH-GRADIENT TEST RESULTS ON A QUADRANT-TYPE X-BAND SINGLE-CELL STRUCTURE

Tetsuo Abe*, Toshikazu Takatomi, Toshiyasu Higo, Shuji Matsumoto, and Yoshio Arakida
High Energy Accelerator Research Organization (KEK), Tsukuba, Japan

Abstract

A common normal-conducting high-gradient accelerating structure of particle accelerators is the "disk type", which has dozens of machined, stacked, and bonded disks. In the disk type, surface currents associated with a magnetic field of an accelerating mode flow across disk-to-disk junctions. Another structure is the "quadrant type", which is *orthogonal* to the above type. In the quadrant type, bonding planes are parallel to a beam axis, and therefore, this type has the remarkable feature that no such surface current flows across any junction. We have proposed, designed, fabricated, and tested an *improved* quadrant-type X-band (11.4 GHz) single-cell structure, and then demonstrated its efficacy and the potential for this structure to be successful for gradients of 100 MV/m or higher at sufficiently low breakdown rates.

INTRODUCTION

High-gradient accelerating structures with gradients of 100 MV/m or higher are indispensable for future high-energy accelerators to search for new physics in particle physics, and are also useful to make compact accelerators of medical linacs and XFELs. Most of these structures, made of oxygen free copper, are fabricated by machining and stacking dozens of disks, and then bonding them by diffusion bonding or brazing ("disk-type" structures). An example of the disk-type structure is shown in Fig. 1a. Disk-type accelerating structures have the potential problem that surface currents associated with a magnetic field of an accelerating mode flow across disk-to-disk junctions, where perfect bonding of neighboring disks at the inner surface is not guaranteed by any bonding method. For example, one report [1] observed small gaps between the diffusion-bonded disks together with some microscopic objects in the SEM images. Although we do not know the details of the radio-frequency (RF) breakdown mechanism that is a dominant contributor to the breakdown rates of accelerating structures, such defects are a serious concern because huge surface currents of $\approx 10^8$ A/cm^2 or higher during high-gradient operations flow across disk-to-disk junctions. Furthermore, a significant impact of the surface magnetic field on breakdown rates has been discovered [2, 3].

Another structure type is the "quadrant type" ("half type" in the case of undamped structures), which is *orthogonal* to the disk type. For quadrant-type structures, no surface current associated with a magnetic field flows across any junction except for perturbative effects. In addition, we
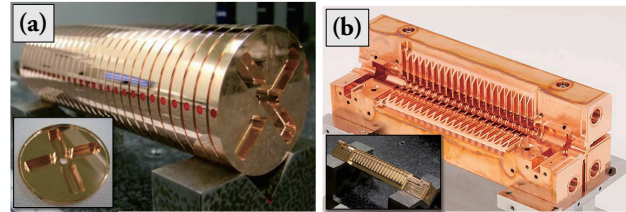

Figure 1: Two types of orthogonal high-gradient accelerating structures: (a) disk type and (b) quadrant type.

can expect significant cost reduction in quadrant-type structure fabrication with simpler machining and bonding compared to disk-type structures. Furthermore, this structure is easy to fabricate from hard materials (e.g., CuAg) without a high-temperature process by using only electron-beam welding (EBW) to maintain its material hardness. This fabrication process is important because it has been found that we can achieve lower breakdown rates for structures with higher yield strength [4].

In 2008, we fabricated a quadrant-type X-band accelerating structure, made of CuZr, with a higher-order-mode (HOM) damped structure by waveguides (waveguide damped structure) consisting of 18 cells (Fig. 1b) [5]. In 2009, we performed a high-gradient test of the structure at KEK/Nextef/Shield-A. As a result, however, the accelerating gradient (E_{acc}) was limited to 60 MV/m or lower with a 50 ns rectangular pulse, and we observed no conditioning effects [6]. SLAC also performed the same type of test, and obtained the same result even with electropolishing of the structure. Usually, we reach E_{acc} = 100 MV/m in RF conditioning of X-band accelerating structures even with a waveguide damped structure. Therefore, such a quadrant-type structure has some fatal flaws.

Although we could not find any evidence, including the material properties of CuZr, for the fatal flaws experimentally, we proposed an *improved*-quadrant-type structure [7, 8] based on simulation studies [9] to overcome all disadvantages of the *naive* quadrant-type design. The new design has the following two key characteristics:

- A large round chamfer of 0.4 mm at the corner of quadrants is added to suppress field enhancements down to +25% for any actual case, where +20% enhancement is a theoretical minimum for any quadrant-type structure, and
- A small finite gap of 0.1 mm between neighboring quadrants is added to avoid any virtual leak.

The chamfer of 0.4 mm and the gap of 0.1 mm are the results of optimization by simultaneously minimizing the field enhancements and deterioration of the shunt impedance ($\approx$

* tetsuo.abe@kek.jp

0.2%). To demonstrate the performance, we fabricated an X-band structure based on the new design in the form of a single-cell standing-wave test cavity [10]. This structure consists of three cells, which are coupling, test, and end cells, as shown in Fig. 2a, where the resonant frequencies of the coupling and end cells are slightly detuned so that the strength of the excited field in the test cell is approximately twice those in the coupling and end cells, as shown in Fig 2b. The coupling and end cells are necessary to make the excited field in the test cell similar to those in a corresponding multi-cell accelerating structure. In other words, this type of single-cell structure with three cells is a minimal structure keeping a realistic RF field for acceleration. It should be noted that single-cell structures are much easier to fabricate and test than multi-cell structures, and therefore, are suitable for basic studies by high-gradient testing.

In this paper, we present results of the high-gradient test of the improved-quadrant-type X-band (11.4 GHz) single-cell standing-wave structure made of oxygen free copper (class1) shown in Figs. 2c-e. The design of the test cell is based on the CLIC prototype structure *TD24R05* [11], which has a waveguide damped structure and is close to the final design for CLIC [12]. It should be noted that a waveguide damped structure is promising for HOM damping in a high-beam current and/or multi-bunch acceleration such as that in linear colliders. This high-gradient test was performed at KEK/Nextef/Shield-B [13] from January 30 to March 24, 2017, all day with around-the-clock operation.

RF MEASUREMENT

Before the high-gradient test, we performed low-power RF measurements. After mounting a SLAC mode converter [14] onto the test cavity, as shown in Fig. 3a, we measured the reflection coefficient (S_{11}) by using a network analyzer, and found no resonance other than the three modes of 0, $\pi/2$, and π in the 11.0 to 11.7 GHz range, as shown in Fig. 3b. We also found perfect matching at the resonance of the accelerating π mode, as shown in the inset of Fig. 3b. The measured resonance frequency and unloaded quality factor are 11.422 GHz (for a cavity temperature of 30°C and vacuum inside) and 7531 (= 95%IACS), respectively. The measured unloaded quality factor is as expected from ultraprecision five-axis milling with carbide tools.

Because the measured frequency (11.422 GHz) and the field-strength pattern are close to the design values (11.424 GHz and green plots in Fig. 4b, respectively), we proceeded to install this test structure into Shield-B, without frequency tuning, on January 23, 2017. It should be noted that the small difference between the measurement and the design shown in Fig. 4b is taken into account in the E_{acc} calculated from the measured RF power (2.5% increase in E_{acc} estimation).
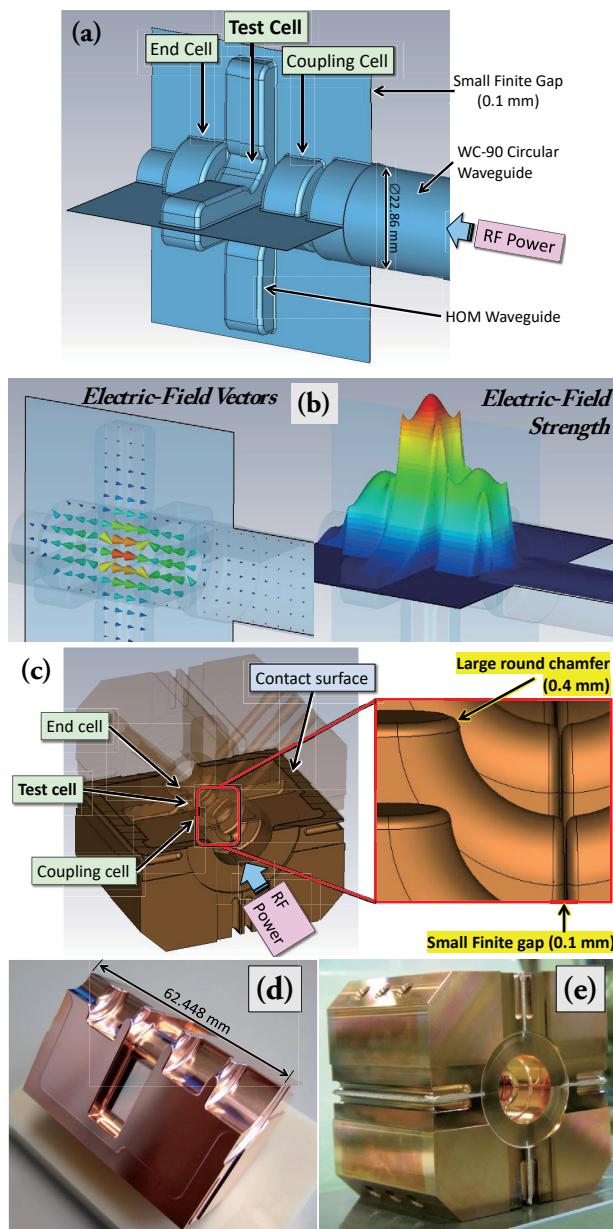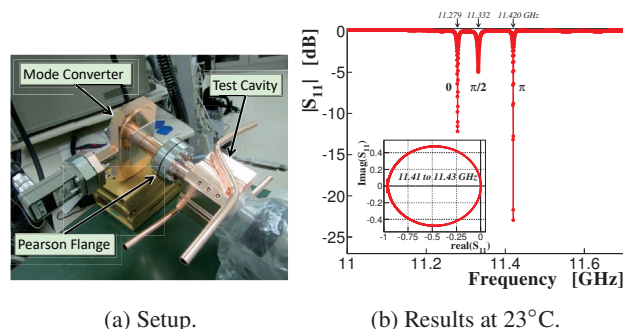

Figure 2: Improved-quadrant-type single-cell structure tested at Shield-B. (a) Electrical design. (b) Electric field of the accelerating π mode. (c) Mechanical design. (d) One of the quadrants machined by ultraprecision five-axis milling. (e) After bonding of the four quadrants by EBW.

(a) Setup. (b) Results at 23°C.

Figure 3: Measurement of the reflection coefficient S_{11}.
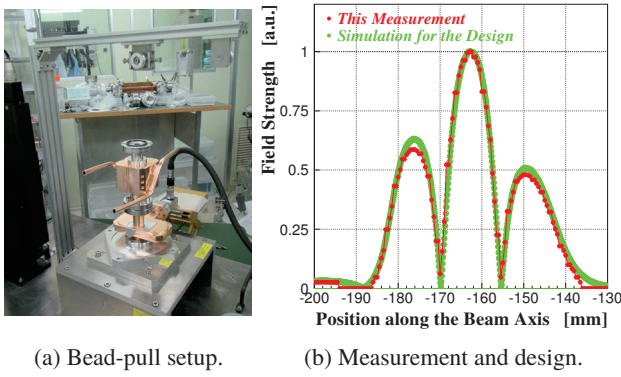
(a) Bead-pull setup. (b) Measurement and design.

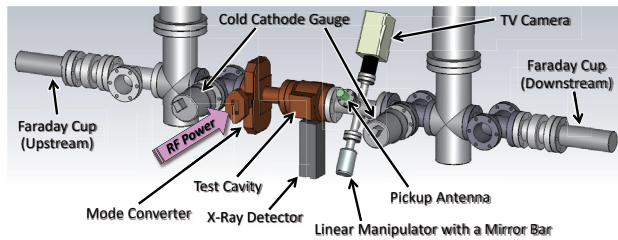Figure 4: Measurement of the field strength.

Figure 5: Experimental setup in Shield-B.

EXPERIMENTAL SETUP

Figure 5 shows the experimental setup in Shield-B. RF high power of 11.4 GHz was fed into the test cavity via the mode converter. More details are described in [13].

To have a constant high field in the test cell as long as possible, we modulated the input RF pulse into two steps as shown in Fig. 6a. In the first step for 100 ns, we charged the RF energy in the test cavity ("charging step"). At the end of the charging step, we suddenly decreased the RF power to approximately one third of that in the charging step so that we could maintain a constant RF field for 150 or 300 ns in the second step ("maintaining step"), as shown in Fig. 6b. By defining $P_{inp}^{(1st)}$ ($P_{inp}^{(2nd)}$) as the RF power input to the test cavity in the charging (maintaining) step, the ratio of $P_{inp}^{(2nd)}/P_{inp}^{(1st)}$ was adjusted so that the reflection level in the maintaining step was minimum.

Breakdown candidate events were triggered by detecting the current flash by the Faraday cups or the pickup antenna, or by an abnormality in the reflection waveform ("reflection-waveform trigger" [13]).

BREAKDOWN CANDIDATES

We define *normalized maximum reflection-waveform difference* ($\tilde{R}_{diff}^{(max)}$) as $\tilde{R}_{diff}^{(max)} = R_{diff}^{(max)}/R^{(max)}$, where $R^{(max)}$ is defined as the peak pulse height in the reflection waveform of a *normal pulse*, and $R_{diff}^{(max)}$ is defined as the maximum absolute value in the difference between the reflection waveform of the breakdown candidate and that of the normal pulse after adjusting the timing when the pulse starts and normalizing the pulse height so that the input RF powers are the same for both. The normal pulse is defined as
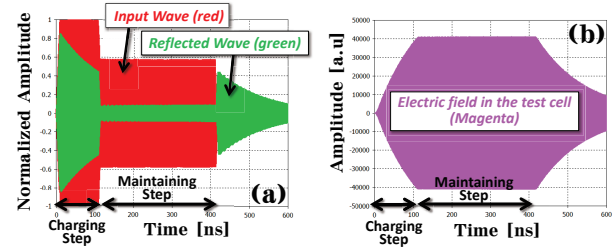

Figure 6: Time-domain simulation using CST MICROWAVE STUDIO with a 11.42-GHz monochromatic input wave for a full model including the mode converter. (a) Input and reflected waves, both of which are normalized so that the amplitude of the input wave in the charging step is one. (b) Electric field excited in the test cell for the input wave in (a).

the average waveform of the last three pulses but seven [1] if such three pulses exist; if such three pulses do not exist, the same procedure is taken for the previous breakdown-candidate event. Figure 7a shows the distributions of $\tilde{R}_{diff}^{(max)}$ for non-breakdown events and breakdown candidates in the step-pulse operation with 100 ns width in the charging step and 150 ns in the maintaining step (100 + 150 ns width). At $\tilde{R}_{diff}^{(max)} = 0.24$, shown in Fig. 7a with a green arrow, non-breakdown events and breakdown candidates can be well separated. We also learn from Fig. 7a that few breakdown candidates with the current flash were found either upstream or downstream (only ≈ 15 %). Several events with $\tilde{R}_{diff}^{(max)} < 0.24$ and the current flash were detected; in those events, the RF pulses for breakdown are missing in an oscilloscope, or noise was detected by the pickup antenna or Faraday cup.

We also define *breakdown timing* (T_{BD}) as the time when such difference in the reflection waveforms starts relative to the time when the reflection of the normal pulse starts, as shown in Fig. 8. Figure 7b shows the two-dimensional distribution of $\tilde{R}_{diff}^{(max)}$ as a function of T_{BD} for current-flash breakdown candidates in the 100 + 150 ns step-pulse operation. There are events with $T_{BD} > 250$ ns (after the maintaining-step period) around $\tilde{R}_{diff}^{(max)} = 0.6$, which are to be excluded from the final breakdown candidates.

As final breakdown candidates in the 100 + 150 ns step-pulse operation, we selected the following:

- Events with $T_{BD} < 250$ ns and current flash detected both upstream and downstream, and
- Events with $T_{BD} < 250$ ns and $\tilde{R}_{diff}^{(max)} > 0.24$.

It should be noted that we detected 504 breakdown candidates with $\tilde{R}_{diff}^{(max)} > 0.24$ in the 100 + 150 ns step-pulse operation by the trigger system, and only 36 of the 504 events had no current flash detected by any Faraday cup or pickup antenna.

RF CONDITIONING

The RF conditioning history is shown in Fig. 9. We started RF conditioning with the 100 ns rectangular pulse up

---

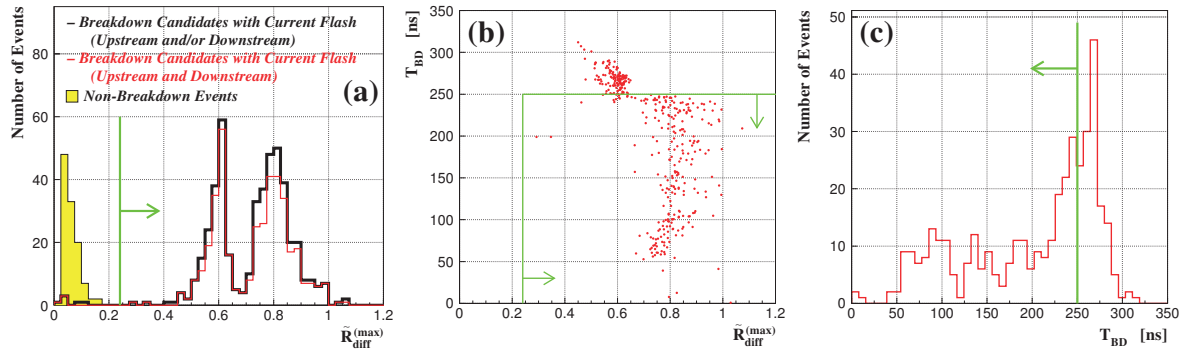[1] Last pulse is defined as a pulse of the breakdown candidate.

Figure 7: Event selection for the 100 + 150 ns step-pulse operation, where the green arrows show the criteria for breakdown candidates.
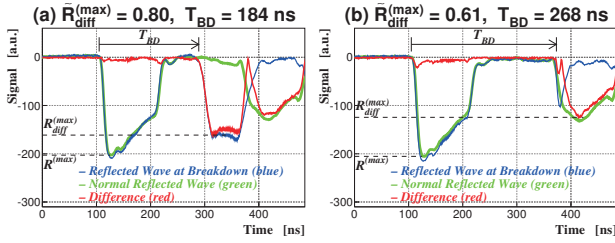

Figure 8: Examples of reflection waveforms.

to $E_{acc} \approx 125$ MV/m. Then we switched to a 100 + 150 ns step-pulse operation up to $E_{acc} \approx 125$ MV/m. This pulse width corresponds to the RF pulse for CLIC (156 ns flat-top, 240 ns full length). Finally, we performed a step-pulse operation with 100 + 300 ns width up to $E_{acc} \approx 125$ MV/m. This RF conditioning proceeded smoothly. It should be noted that the target gradient of $E_{acc} \approx 125$ MV/m was not the performance limit; the limiting factor was the time limit of the high-gradient test. We observed a further conditioning effect even at $E_{acc} \approx 125$ MV/m with 100 + 300 ns width.

BREAKDOWN-RATE MEASUREMENT

After the RF conditioning, we performed breakdown-rate measurement with 100 + 150 ns width based on the *cycle* operation. The cycle operation consists of four power levels: $P_{inp}^{(2nd)}$ = 5.4, 5.0, 4.2, and 3.5 MW, which correspond to E_{acc} = 125, 120, 110, and 100 MV/m, respectively. One cycle contained the following sequential procedure: 1. Increasing the RF power up to $P_{inp}^{(2nd)}$ = 5.4 MW; 2. Maintaining $P_{inp}^{(2nd)}$ = 5.4 MW by feedback control for elapse time 5 min only for RF conditioning; 3. Decreasing the RF power down to $P_{inp}^{(2nd)}$ = 5.0 MW; 4. Maintaining $P_{inp}^{(2nd)}$ = 5.0 MW by feedback control for elapse time 60 min; 5. Decreasing the RF power down to $P_{inp}^{(2nd)}$ = 4.2 MW; 6. Maintaining $P_{inp}^{(2nd)}$ = 4.2 MW by feedback control for elapse time 120 min; 7. Decreasing the RF power down to $P_{inp}^{(2nd)}$ = 3.5 MW; and 8. Maintaining $P_{inp}^{(2nd)}$ = 3.5 MW by feedback control for elapse time 240 min.
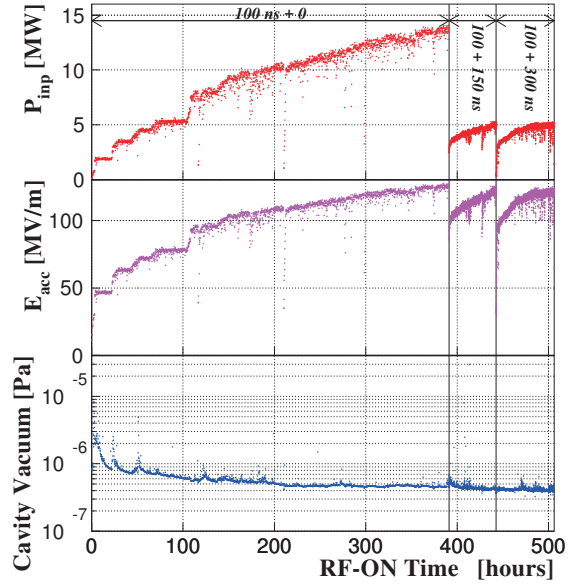

Figure 9: RF conditioning history using a 100 ns rectangular pulse, 100 + 150 ns and 100 + 300 ns step pulses until E_{acc} reached ≈ 125 MV/m, where E_{acc} indicates the maximum gradient during the 100 ns rectangular pulse, or the gradient during the maintaining step of the step pulse. P_{inp} indicates $P_{inp}^{(1st)}$ for the rectangular pulse, or $P_{inp}^{(2nd)}$ for the step pulses.

We counted all of the input RF pulses, which reached a total of 39749237 for the constant-power periods, using an oscilloscope (Tektronix DPO7054C). We also counted the number of breakdowns according to the abovementioned criteria for the constant-power periods. Then, we calculated breakdown rates at E_{acc} = 100, 110, and 120 MV/m, as shown in Fig. 10, for each of the half periods of this measurement. We detected 12 (4) final breakdown candidates in the former (latter) period. These numbers indicate a further conditioning effect during this measurement.

Assuming a power low of (breakdown rate) $\propto E_{acc}^{30}$ [15], we can expect sufficient high-gradient performance of the quadrant type of accelerating structure to meet the CLIC specification [12].
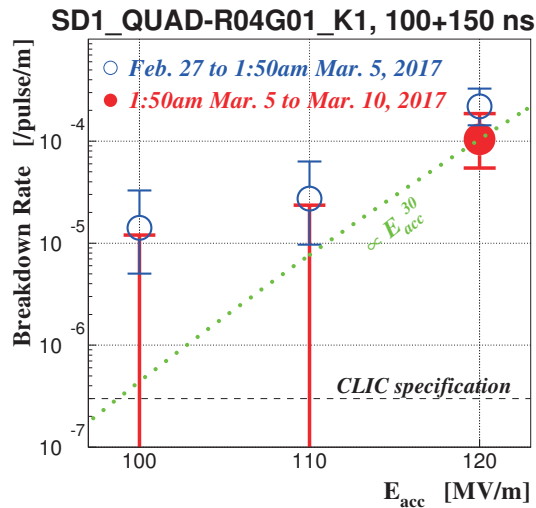
SD1_QUAD-R04G01_K1, 100+150 ns

Figure 10: Results of this breakdown-rate measurement. The error bars indicate a 1σ confidence interval. No breakdown candidates were detected at $E_{acc} = 100$ and 110 MV/m in the latter half period; therefore, only the statistical upper limits are shown for a 1σ confidence interval (assuming 1.841 events in average at $E_{acc} = 100$ or 110 MV/m).

OTHER REMARKS AND CONCLUSIONS

We have proposed, designed, fabricated, and tested the improved-quadrant-type X-band single-cell standing-wave structure. During the RF conditioning, even for the 100 + 300 ns pulse width, E_{acc} smoothly reached 125 MV/m. This value of E_{acc} is much higher than the highest gradient of 60 MV/m in the high-gradient test of the 18-cell naive-quadrant-type X-band traveling-wave accelerating structure for the 50 ns rectangular pulse. We observed a further conditioning effect even at $E_{acc} \approx 125$ MV/m, and no performance limit. Therefore, we have demonstrated the possibility of succeeding with this fabrication method based on the quadrant type.

Throughout this high-gradient test, we observed no light, by the TV camera and mirror, in the small finite gap of 0.1 mm between quadrants except for breakdown timings, and no serious problem related to the gap. Therefore, we also have demonstrated that a small gap can withstand high fields if the frequencies of all the eigenmodes inside the small gap are adequately controlled [8].

From this breakdown-rate measurement, we can expect sufficient high-gradient performance of the quadrant type of accelerating structure to meet the CLIC specification (3 $\times 10^{-7}$ breakdowns/pulse/m) at 100 MV/m.

Our next step is to fabricate and test the 24-cell CLIC prototype *TD24R05* (traveling wave) [11] with this fabrication method based on the quadrant type as a complete demonstration of its principle and efficacy.

ACKNOWLEDGMENTS

REFERENCES

[1] M. Aicherer, "TD18 post-mortem SEM observation: Update," tech. rep., CERN, November 2010. CERN EDMS.

[2] V. Dolgashev *et al.*, "Geometric Dependence of Radio-Frequency Breakdown in Normal Conducting Accelerating Structures," *Appl. Phys. Lett.*, vol. 97, p. 171501, 2010.

[3] F. Wang *et al.*, "Performance limiting effects in X-band accelerators," *Phys. Rev. ST Accel. Beams*, vol. 14, p. 010401, 2011.

[4] V. A. Dolgashev, "High Gradient, X-Band and Above, Metallic RF Structures," in *the 2nd European Advanced Accelerator Concepts Workshop, Italy*, 2015.

[5] T. Higo *et al.*, "Fabrication of a Quadrant-type Accelerator Structure for CLIC," *Conf. Proc.*, vol. C0806233, 2008.

[6] T. Higo, "KEK activities on CLIC X-band Accelerating Structures." CERN Indico, March 2010. Presented in Mini-Workshop on CLIC X-band Structure R&D at THU.

[7] T. Abe *et al.*, "Quadrant-Type X-Band Single-Cell Structure for High Gradient Tests," in *Proceedings of the 9th Annual Meeting of Particle Accelerator Society of Japan*, 2012. THPS095 (Japanese).

[8] T. Abe *et al.*, "Fabrication of Quadrant-Type X-Band Single-Cell Structure used for High Gradient Tests," in *Proceedings of the 11th Annual Meeting of Particle Accelerator Society of Japan*, 2014. SUP042.

[9] T. Abe, "Study of Surface Field Enhancements due to Fine Structures," in *Proceedings of the 8th Annual Meeting of Particle Accelerator Society of Japan*, 2011. TUPS086.

[10] V. A. Dolgashev *et al.*, "Travelling wave and standing wave single cell high gradient tests," in *Linac 2004*.

[11] T. Higo *et al.*, "Comparison of High Gradient Performance in Varying Cavity Geometries," in *IPAC 2013*. WEPFI018.

[12] M. Aicheler *et al.*, "A Multi-TeV Linear Collider Based on CLIC Technology : CLIC Conceptual Design Report," *CERN-2012-007*, 2012.

[13] T. Abe *et al.*, "High-Gradient Testing of Single-Cell Test Cavities at KEK / Nextef," in *Proceedings of the 13th Annual Meeting of Particle Accelerator Society of Japan*, 2016. MOP015.

[14] C. Nantista *et al.*, "Low-field accelerator structure couplers and design techniques," *Phys. Rev. ST Accel. Beams*, vol. 7, p. 072001, 2004.

[15] A. Grudiev *et al.*, "New local field quantity describing the high gradient limit of accelerating structures," *Phys. Rev. ST Accel. Beams*, vol. 12, p. 102001, 2009.